Eur. Phys. J. B **8**, 169–177 (1999)

THE EUROPEAN PHYSICAL JOURNAL B

EDP Sciences

Structural study of the ferroelectric instability in $Sn_2P_2Se_6$

R. Enjalbert[1], J. Galy[1], Y. Vysochanskii[2], A. Ouédraogo[3], and P. Saint-Grégoire[4,a]

[1] CEMES-CNRS[b], B.P. 4347, 31055 Toulouse Cedex, France
[2] Department of Physics and Chemistry of Solid State, Uzhgorod State University, 294000 Uzhgorod Ukraine
[3] Université de Ouagadougou, FAST, Ouagadougou, Burkina
[4] Université Toulon-Var, Bâtiment R, B.P. 132, 83957 La Garde Cedex, France

Received: 10 July 1998

Abstract. The structural change occurring in $Sn_2P_2Se_6$ between the paraelectric and the ferroelectric phases is investigated by means of X-ray diffraction. Details of the structure in both phases are obtained and the role of the Sn^{2+} lone pair is discussed in the light of structural data. In agreement with the $2/m$ to m symmetry lowering, polar displacements are found within the m plane away from a particular crystallographic direction but antiparallel displacements occur also. These results are discussed in the frame of the phenomenological theory which predicts a particular temperature dependence of the dielectric polarization in this crystal.

PACS. 61.10.Nz Crystal structure solution and refinement techniques using X-rays – 64.70.Rh Solid-solid transitions – 77.80.-e Ferroelectricity and antiferroelectricity

1 Introduction

$Sn_2P_2X_6$ (X = S, Se) compounds, which undergo a phase transition with a symmetry reduction from $2/m$ to m, are particularly interesting both from applied and fundamental physics in relation with their semiconducting and ferroelectric properties. They form solid solutions and in the phase diagram a Lifshitz point and a tricritical point are encountered [1,2]. Hence, $Sn_2P_2Se_6$ presents an intermediate incommensurate (IC) phase, $Sn_2P_2S_6$ undergoes directly the transition to the uniaxial ferroelectric phase, and in the solid solution Sn_2P_2 $(Se_xS_{1-x})_6$ the modulation wave vector vanishes and the intermediate IC phase disappears for a composition near $x = 0.28$, which defines the Lifshitz point [3,4]. The phase transitions in this family of compounds have a displacive character evidenced by light [5] and neutron scattering [6] studies. However in the neighbourhood of the transition point the modes become overdamped and central peaks are found [7], which could indicate a slight order-disorder character.

In contrast with the large amount of studies only few structural studies have been performed [8–11]. In $Sn_2P_2S_6$ a model has been proposed on the basis of analysis of phonon modes [12]; the deduced atomic displacements connected with the transition – a Sn^{2+} translation along a crystallographic axis – has been confirmed by X-ray structure resolution at low temperature. In the Se compound the structural arrangement in the IC phase has been analyzed qualitatively [4].

The aim of the present paper is to show the results concerning the differences of structure between paraelectric and ferroelectric phases of $Sn_2P_2Se_6$ as obtained by means of analysis of X-ray diffraction data, and to discuss them in connection with the existence of the intermediate IC phase in this compound. The structure of paraelectric phase was previously determined by Voroshilov *et al.* [10], but we reinvestigated it to compare more safely the structures of the high and low temperature phases. During the present work a paper by Israel *et al.* appeared on the same subject [11], showing results in good agreement with those presented here. The small differences can be understood on the basis of data presented in Figure 1 since results of reference [11] were obtained at a different temperature in the ferroelectric phase. In the present study we focus however on different aspects in relation with the structural properties: on the role of the lone pair associated with Sn^{2+} on one hand, and on the symmetry properties of the system, discussed in the light of a phenomenological approach.

2 Experimental

Single crystals were obtained by a vapour transport technique [13] at the Institute of Solid State Physics and Chemistry at Uzhgorod University. The X-ray data collection has been performed with a Nonius CAD4 diffractometer equipped with a low temperature device. The cooling was achieved by means of a temperature regulated cold nitrogen jet, directed onto the sample. The temperature

[a] e-mail: `streg@univ-tln.fr`
[b] UP – CNRS 8011

Table 1. Crystallographic parameters of PE and FE phases

Crystal data		
	PE phase	FE phase
Crystal system	monoclinic	monoclinic
Temperature (K)	293	150
Space group	$P2_1/n$	Pn
a (Å)	6.815(1)	6.805(1)
b (Å)	7.671(3)	7.708(2)
c (Å)	9.626(4)	9.616(5)
$\beta(^\circ)$	91.01(4)	91.03(5)
V (Å^3)	503.2(3)	504.4(3)
Z	2	2
Molecular weight	773.08	773.08
ρ_{calc} (g cm^{-3})	5.10	5.09
μ (MoKα cm^{-1})	269	268
Morphology	block	block
Dimension (mm)	$0.15 \times 0.125 \times 0.088$	$0.15 \times 0.125 \times 0.088$
Data collection		
Wavelength [MoKα] (Å)	0.71069	0.71069
Monochromator	graphite	graphite
Scan mode	ω-2θ	ω-2θ
Scan width ($^\circ$)	$0.90 + 0.35 \tan\theta$	$0.80 + 0.35 \tan\theta$
Take-off angle ($^\circ$)	4.0	4.0
Range of hkl	$h: 0 \rightarrow 8$, $k: 0 \rightarrow 9$, $l: -11 \rightarrow 11$	$h: 0 \rightarrow 8$, $k: 0 \rightarrow 9$, $l: -12 \rightarrow 12$
Max Bragg angle ($^\circ$)	25	27
Time max. (s)	60	60
Control reflections		
Intensity (every 3600 s)	$00\overline{4}$ / $22\overline{2}$ / $\overline{6}00$	060 / 006 / 082
Orientation (every 150 reflections)	$\overline{6}02$ / $6\overline{2}0$	$11\overline{3}$ / $31\overline{5}$
Structure refinement		
Reflections collected	778	1050
Refinement on F^2:		
Reflections unique used	683	985
R_{int}	0.028	0.039
Parameters refined	47	90
Secondary extinction	0.013(2)	0.008(1)
$R = \sum \parallel F_o \mid - \mid F_c \parallel / \sum \mid F_o \mid$	0.053	0.049
$wR = [\sum w(\mid F_o \mid - \mid F_c \mid)^2 / \sum wF_o^2]^{\frac{1}{2}}$	0.142	0.133
Weighting w^{-1}	$\sigma^2(F_o^2) + 0.1\ P^2$	$\sigma^2(F_o^2) + 0.1\ P^2 + 5.6\ P$
	$P = (F_o^2 + 2F_c^2)/3$	$P = (F_o^2 + 2F_c^2)/3$
Goodness of fit S	1.25	1.06
ρ_{max}/ρ_{min} (e/Å^3)	2.49 / -1.62	2.86 / -2.49

was measured by means of a chromel-alumel thermocouple situated within the tube driving the gas, the extremity of which is at 4 mm from the sample, and thereafter corrected by performing a linear interpolation (the correction is smaller than 2 K) after locating the lock-in phase transition (193 K) from the thermal behaviour of the lattice parameters (Fig. 1) (cell parameters were determined from recording 25 hkl reflections). The temperature accuracy is then about 1 K. X-ray data collections were then performed at 293 K and at 150 K; details are summarized in Table 1.

Intensities were corrected for Lorentz polarization factors and absorption [14]. The atomic scattering factors were corrected for anomalous dispersion [15]. Calculations and drawings were performed using SHELX [16] and ORTEP [17] softwares.

Table 2. Coordinates and thermal atomic parameters of PE and FE phases

$T = 293$ K						
Atom	x	y	z	U_{eq} (Å^2)		
Sn	0.4618(2)	0.3751(2)	0.2465(2)	0.0412(6)		
P	0.4396(5)	0.1056(5)	0.5644(4)	0.0099(9)		
Se1	0.6640(2)	0.3085(2)	0.5562(2)	0.0147(5)		
Se2	0.3903(2)	−0.0075(2)	0.7693(1)	0.0155(5)		
Se3	0.1721(2)	0.1983(2)	0.4584(1)	0.0145(5)		
Atom	U_{11}	U_{22}	U_{33}	U_{23}	U_{13}	U_{12}
Sn	0.0334(8)	0.028(1)	0.062(1)	−0.0015(7)	0.0078(6)	0.0015(6)
P	0.013(2)	0.009(2)	0.008(2)	−0.000(1)	0.002(1)	0.001(1)
Se1	0.0188(8)	0.011(1)	0.0141(8)	0.0012(6)	0.0002(6)	−0.0019(6)
Se2	0.0225(8)	0.016(1)	0.0078(7)	0.0018(6)	0.0031(6)	0.0057(6)
Se3	0.0158(8)	0.016(1)	0.0115(8)	0.0002(6)	0.0002(5)	0.0021(6)
$T = 150$ K						
Atom	x	y	z	U_{eq} (Å^2)		
Sn1	0.44	0.6215(2)	0.25	0.0142(5)		
Sn2	0.4992(3)	−0.1314(3)	0.7540(2)	0.0130(4)		
P1	0.4035(9)	0.3539(9)	0.5367(6)	0.0061(12)		
P2	0.5255(9)	0.1445(8)	0.4068(6)	0.0046(11)		
Se1	0.6183(5)	0.5592(3)	0.5255(3)	0.0073(5)		
Se2	0.3522(4)	0.2438(3)	0.7423(3)	0.0080(5)		
Se3	0.1324(4)	0.4445(3)	0.4279(3)	0.0066(5)		
Se4	0.2919(5)	−0.0563(3)	0.4166(3)	0.0074(5)		
Se5	0.5667(4)	0.2595(3)	0.2031(3)	0.0074(5)		
Se6	0.7904(5)	0.0512(3)	0.5080(3)	0.0081(5)		
Atom	U_{11}	U_{22}	U_{33}	U_{23}	U_{13}	U_{12}
Sn1	0.0174(10)	0.0098(8)	0.0158(8)	0.0039(7)	0.0022(7)	−0.0002(8)
Sn2	0.0123(9)	0.0119(9)	0.0149(8)	−0.0008(7)	0.0023(6)	0.0002(7)
P1	0.004(3)	0.006(3)	0.009(3)	−0.000(2)	−0.003(2)	0.002(2)
P2	0.010(3)	0.001(3)	0.003(3)	0.001(2)	−0.001(2)	0.000(2)
Se1	0.0096(12)	0.0052(11)	0.0070(11)	0.0002(8)	−0.0004(8)	−0.0008(9)
Se2	0.0104(12)	0.0086(12)	0.0052(10)	0.0010(9)	0.0023(8)	0.0021(10)
Se3	0.0069(12)	0.0053(12)	0.0076(11)	0.0009(8)	−0.0001(8)	0.0007(9)
Se4	0.0092(11)	0.0040(11)	0.0090(11)	0.0001(8)	0.0007(8)	−0.0022(9)
Se5	0.0129(13)	0.0047(11)	0.0046(10)	0.0008(8)	0.0010(8)	0.0030(9)
Se6	0.0091(12)	0.0091(13)	0.0061(10)	0.0007(8)	−0.0007(8)	0.0020(9)

3 Results

3.1 Room temperature structure

Structures were determined in the monoclinic system. At 293 K there are two possible choices for the label of the space group, namely $P2_1/n$ and $P2_1/c$. In order to have angles close to 90° we have selected the former. At 150 K the symmetry is Pn. Final values of refinements are presented in Table 1, positional and thermal parameters in Table 2, and main distances and angles in Table 3.

The structure at 293 K was reinvestigated only in order to have a more reliable reference for comparing the ferroelectric and paraelectric phases, since they were determined in the same conditions. Our results at room temperature (Fig. 2a) are in good agreement with those of Voroshilov *et al.* [10] and Israël *et al.* [11]. The $[P_2Se_6]$ groups are disposed in coordination octahedra (Fig. 2b) and the Sn^{2+} atoms are surrounded by eight Se atoms forming a bicapped trigonal prism (BTP) (Fig. 2c). Octahedra containing a couple of P atoms are connected by empty octahedra and form chains along the [101] and $[\overline{1}01]$ directions.

Table 3. Selected interatomic distances (Å) and angles (°) in both phases

293 K					
P					
Se1	2.183(4)				
Se2	2.187(4)	115.8(2)			
Se3	2.191(4)	109.3(2)	114.0(2)		
Pa	2.213(8)	103.6(2)	106.1(3)	106.9(2)	
	P	Se1	Se2	Se3	
$\overline{\text{P}-\text{Se}} = 2.187$					
Sn					
Se2a	2.999(2)				Symmetry code:
Se1b	3.054(2)				a: $-x+1$, $-y$, $-z+1$
Se2c	3.096(2)				b: $x-\frac{1}{2}$, $-y+\frac{1}{2}$, $z-\frac{1}{2}$
Se3	3.169(2)				c: $x+\frac{1}{2}$, $-y+\frac{1}{2}$, $z-\frac{1}{2}$
Se3c	3.194(2)				d: $-x+1$, $-y+1$, $-z+1$
Se1d	3.207(2)				e: $-x+\frac{1}{2}$, $y+\frac{1}{2}$, $-z+\frac{1}{2}$
Se3e	3.287(2)				f: $-x+\frac{1}{2}$, $y-\frac{1}{2}$, $-z+\frac{1}{2}$
Se1	3.303(2)				g: $-x$, $-y$, $-z+1$
					h: $-x+1$, $-y$, $-z+1$
$\overline{\text{Sn}-\text{Se}}$ 3.164					
150 K					
P1					
Se1	2.159(7)				
Se2	2.186(6)	116.7(3)			
Se3	2.220(6)	107.5(3)	113.9(3)		
P2	2.211(7)	104.2(3)	107.2(3)	106.5(3)	
	P1	Se1	Se2	Se3	
$\overline{\text{P1}-\text{Se}} = 2.188$					
P2					
Se6	2.157(7)				
Se5	2.173(6)	115.0(3)			
Se4	2.222(7)	110.0(3)	115.2(3)		
P1	2.211(7)	107.9(3)	105.5(3)	102.0(3)	
	P2	Se6	Se5	Se4	
$\overline{\text{P2}-\text{Se}} = 2.184$					
Sn1		Sn2e			
Se1	2.931(3)	Se4	2.897(3)		Symmetry code:
Se5	2.956(3)	Se6h	2.914(3)		a: $x+\frac{1}{2}$, $-y+1$, $z-\frac{1}{2}$
Se2a	2.992(3)	Se2e	3.061(3)		b: x, $y+1$, z
Se3	3.045(3)	Se3	3.070(3)		c: $x-\frac{1}{2}$, $-y+1$, $z-\frac{1}{2}$
Se4b	3.131(3)	Se5h	3.137(3)		d: $x-\frac{1}{2}$, $-y$, $z+\frac{1}{2}$
Se1c	3.353(3)	Se1c	3.355(3)		e: $x-\frac{1}{2}$, $-y$, $z-\frac{1}{2}$
Se3a	3.426(3)	Se6e	3.417(3)		f: $x+\frac{1}{2}$, $-y$, $z+\frac{1}{2}$
Se6c	3.569(3)	Se4e	3.567(3)		g: x, $-y+1$, z
					h: $x-1$, y, z
$\overline{\text{Sn1}-\text{Se}}$ 3.175		$\overline{\text{Sn2}e-\text{Se}}$ 3.177			

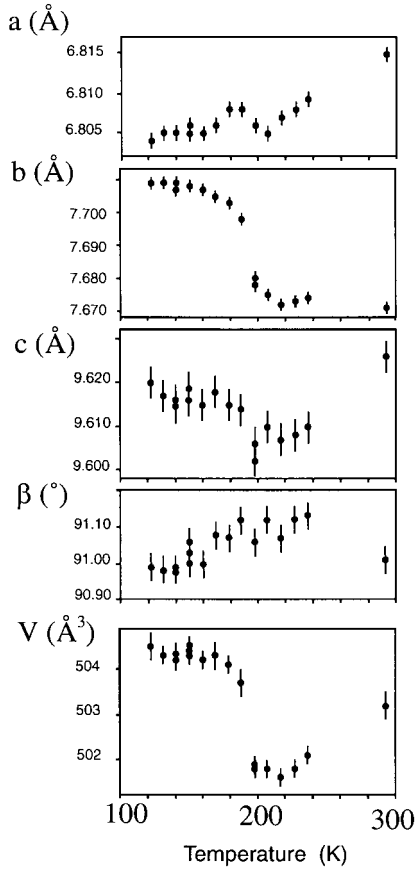

Fig. 1. Evolution of the cell parameters of $Sn_2P_2Se_6$ *versus* temperature.

3.2 Thermal variation of the lattice parameters

Figure 1 presents the thermal variation of the lattice parameters. The systematic determination and refinement of the $Sn_2P_2Se_6$ cell parameters *versus* temperature (down to 122 K) allowed to note remarkable differences in the a, b, c, ß and V evolutions. They are in general agreement with Barsamian *et al.* [4] results which give the interplanar distances d_{001}, d_{010}, d_{101} and d_{100}. On cooling, the crystallographic parameter a decreases until 208 K, then increases until 190 K and decreases again below this temperature. The b parameter after an almost flat evolution until 215 K strongly increases below 200 K and its evolution presents an inflexion point or a jump around 193 K. This increase continues regularly down to the lowest temperatures where we performed measurements. The c parameter decreases below room temperature till the neighbourhood of 200 K and thereafter presents a thermal dependence below 193 K resembling that for b. Above this temperature the plateau found by previous authors related with an invar effect is not so clearly marked but our data between 193 K $\leq T \leq$ 220 K are consistent with it. The angle β shows a smooth evolution. The curve representing the cell volume *versus* T exhibits, after a minimum around 218 K, a drastic increase at 193 K followed by a smooth but again continuous increase down to 122 K. These evolutions can be accounted for as indicated by Barsamian *et al.* [4]

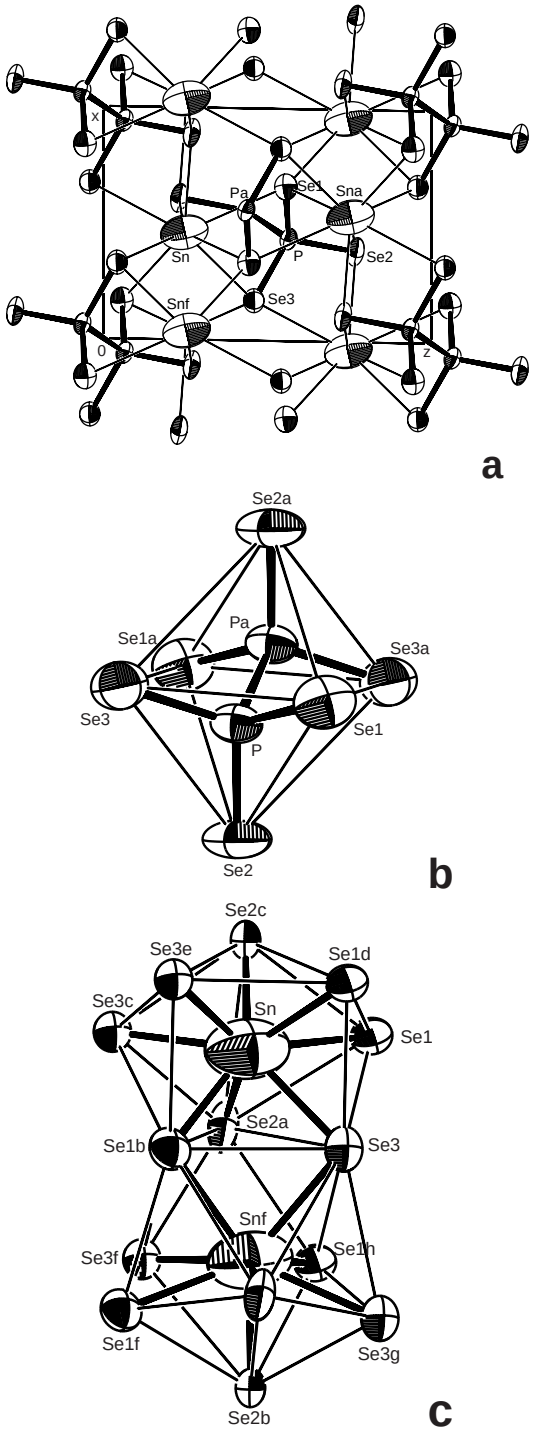

Fig. 2. PE – $Sn_2P_2Se_6$ structure. (a) Projection of the structure onto the (010) plane. (b) P_2Se_6 group. (c) Association of two $SnSe_8$ polyhedra along the [010] direction.

by a second order transition starting around 220 K followed by a first order transition at 193 K with a space group change from centrosymmetric $P2_1/n$ to non centric Pn. Since the variation of the lattice parameters are related to a coupling between the symmetrical components of the strain tensor and the square of the order parameter amplitude (which is invariant) the anomalous part is proportional to P^2; the analysis of the experimental results

on the variation of b shows that this variation follows a dependence $\delta b \propto (T - T_c)^{2\widetilde{\beta}}$ with a value of $\widetilde{\beta} = 0.14 \pm 0.005$, which is in good agreement with a first order phase transition at the lock-in, that can be compared for instance with the value 0.16 in quartz [18]. Such a weak value expresses in fact that the phase transition is of first order and in such a case the thermal dependence of P in the low temperature phase is better described by a Landau-Devonshire law where the coefficient of the quartic term in the free energy expansion is negative [19].

3.3 Structural modifications

Both room temperature (293 K) and low temperature (150 K) final values of the refinement are presented in Tables 1, 2, 3. To make the comparison of both structures easier, we fixed the z-coordinate of Sn1 at 1/4. Structures projected onto the (010) plane are represented in Figures 2a and 3a. They are respectively labelled thereafter as PE$-Sn_2P_2Se_6$ (paraelectric phase) and FE$-Sn_2P_2Se_6$ (ferroelectric phase). Ellipsoids which are shown correspond to a presence probability of 95%. In PE phase, P and Pa are related by inversion; in the FE phase these P atoms which are no more related by inversion are now respectively labelled as $P1$ and $P2$.

The PE $- Sn_2P_2Se_6$ network is built up by $[P_2Se_6]$ groups linked by Sn^{2+} ions. The $[P_2Se_6]$ groups are formed by PSe_3 units associated in pairs *via* a P$-$P coordination bond. The selenium atoms form an octahedron, the two PSe_3 units being exactly in a staggered position (center of symmetry on the P$-$P bond). The $[P_2Se_6]$ octahedron makes the packing denser in the (101) plane owing to the repetition generated by the 2_1 screw symmetry. Finally this $[P_2Se_6]$ octahedra packing form layers leaving empty selenium octahedra. Tin atoms lie in planes parallel to (001), situated at $\frac{1}{4}c$ and $\frac{3}{4}c$ in between the $[P_2Se_6]_n$ layers. They ensure the stability of the structure, each of them interconnecting four $[P_2Se_6]$ groups pertaining to two different $[P_2Se_6]_n$ layers. However, it is to be noted that the strongest bonding occurs in the neighbourhood of the (101) plane, the resulting (101) $[Sn_2P_2Se_6]_n$ layers showing longer bonding in the [101] direction. The detailed bonding scheme of the (P_2Se_6) octahedron is depicted in Figure 2b; all the atoms have large thermal parameters. Therefore all the P$-$Se distances are almost equal, the deviation from the P$-$Se mean value being of the order of the precision, *i.e.* 0.004 Å. The tin atom shows an eightfold coordination, the selenium atoms being at the corners of a bicapped trigonal prism BTP. These $[SnSe_8]$ polyhedra with a 54.9 Å^3 volume share edges and corners in the tin layer parallel to the (001) plane and also with the $[P_2Se_6]$ octahedra. The association of $[SnSe_8]$ polyhedra related by the twofold axis, corresponding to the shortest Sn$-$Sn distance (Sn$-$Sn$_f$ = 4.801 Å), is represented in Figure 2c. The square bases of the trigonal prisms not capped, *i.e.* Se1*b*-Se3-Se1*d*-Se3*e* for Sn and Se1*b*-Se3-Se1*h*-Se3*f* for Sn$_f$, share the Se1*b*-Se3 edge and make an angle of 32.5° which marks the puckering of this layer of bicapped trigonal prisms. Inside its polyhedron the tin atom is highly affected by thermal vibrations. Being in presence of Sn^{2+}, a one sided coordination would be expected, if the E lone pair $5s^2$ was stereochemically active. In fact, even if we note three shorter Sn$-$Se distances around 3 Å (Sn$-$Se1*b*, Sn$-$Se2*a* and Sn$-$Se2*c*) the remaining ones give values in between 3.169 Å and 3.303 Å. The lone pair effect seems to be hidden by the large Sn

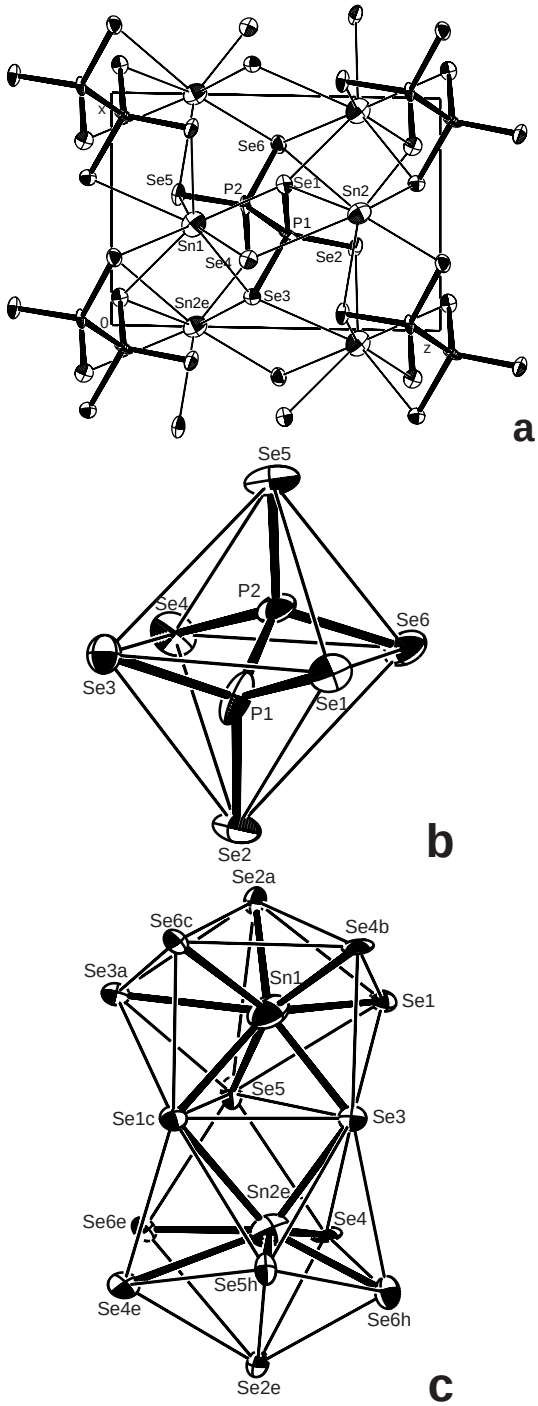

Fig. 3. FE $- Sn_2P_2Se_6$ structure. (a) Projection of the structure onto the (010) plane. (b) P_2Se_6 group. (c) Association of two $SnSe_8$ polyhedra along the [010] direction.

thermal ellipsoid. Following the principles described by Galy *et al.* [20,21] to localize the center of the E sphere of influence which coincides here with the barycenter G_{Se} of the Se_8, we note a displacement $Sn{-}G_{Se}$ of 0.16 Å.

The FE $- Sn_2P_2Se_6$ structure shows a similar general network architecture, but important distortions due to loss of centrosymmetry induce a new coordination bonding scheme. The $[P_2Se_6]$ group exhibits, as it is common in molecules at low temperature, similar P−Se covalent bonds. Nevertheless, if in the FE $- Sn_2P_2Se_6$, $\overline{P1{-}Se} =$ 2.188 Å and $\overline{P2{-}Se} = 2.184$ Å are very close to $\overline{P{-}Se}$ in the PE-form ($\overline{P{-}Se} = 2.187$ Å), there is a significant increase of the maximal deviation from these mean values, *i.e.* 0.04 Å, which is ten times higher than at room temperature (see Tab. 3). Moreover, whereas the [P−Se3] units are still in staggered position, a slight rotation has occurred around the P−P coordination bond indicated by the torsion/dihedral angles Se1-P1-P2-Se4 = −177.8°, Se2-P1-P2-Se5 = 178.7° and Se3-P1-P2-Se6 = 179.8° (Fig. 3b). The most striking difference occurs at the level of the Sn coordination. As indicated in Figure 3c, the thermal ellipsoids of both Sn and Se atoms have been drastically diminished. Both Sn1 and Sn2 are again inserted in selenium bicapped trigonal prisms (roughly with the same volumes, 55.5 $Å^3$ for Sn1 and 55.0 $Å^3$ for Sn2) but the bonding scheme exhibits now the classical one-sided coordination $[SnSe_5]$, the five selenium atoms making a square pyramid (SP) with tin outside and the lone pair E being opposite to its apex (Figs. 4a, 4b). In the two SP $[Sn1Se_5]$ and $[Sn2Se_5]$, *i.e.* [Sn1-Se4*b*-Se2*a*-Se5-Se3-Se1] and [Sn2*e*-Se4-Se2*e*-Se5*h*-Se3-Se6*h*] the respective apices are Se1 and Se6*h*, the Sn−Se bonds ranging from 2.897 Å to 3.137 Å. Sn1 and Sn2*e* distances from the basal square plane are quasi-identical, 0.70 Å and 0.74 Å. The lone pairs E_1 and E_2 are located around the barycentre of the BTP situated at 0.28 Å and 0.40 Å from Sn1 and Sn2*e* respectively; the other long Sn1 or Sn2 interactions with the remaining seleniums of the BTP ranging from 3.355 Å to 3.569 Å. We note that the strengthening of the covalent bonding is uniquely pointing in one direction, along [001]. The lone pair stereo-activity relax the association in the (001) plane of the $[SnSe_8]$ BTP along the [010] direction, involving a noticeable increase of the b parameter. This detailed analysis of the structure shows the remarkable increase of the stereo-activity of the lone pairs associated with the Sn^{2+} atoms. This stereo-activity is hidden at room temperature by the strong thermal vibration of the tin atoms which allows a direct attractive interaction of Sn with the various Se atoms of the polyhedron.

On the other hand, the stereo-activity of the lone pair in the FE form is well directed due to the one sided coordination of the tin atoms, lowering considerably the Sn−Se attractions with a correlative increase of the remaining Sn−Se interatomic distances up to 3.60 Å (maximum Sn−Se in the PE-form 3.30 Å). Such facts could be responsible for the phase transition occurring at 193 K, this temperature corresponding to a sufficient decreasing of the vibronic effects to allow the lone pairs E of Sn^{2+} to dictate their stereo-activity which lowers the symmetry of the cell. The drastic structural changes so induced can be directly related with the ferroelectric-paraelectric transition and we do believe that this lone pair effect is really the driving force of this physical property. The stereo-activity of the lone pairs in oxides is always marked while in several S and Se compounds it is less obvious. Note that the selenium size is quite important compared with that of oxygen, making polyhedra rather large and therefore allowing huge movements of the lone pair element, here the tin atoms. In SnO, isostructural with PbO, the tin coordination is clearly fivefold even above room temperature, with a one sided SnO_5 square pyramid. In the present case of $Sn_2P_2Se_6$ it is necessary to cool the material down to the point where the lone pair effect becomes more important than vibronic effects.

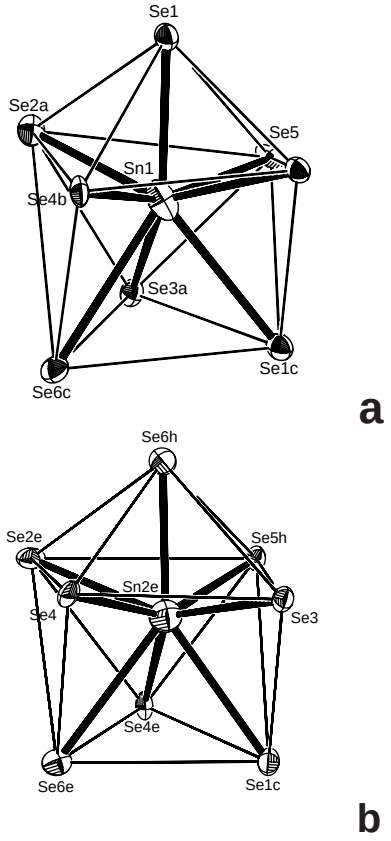

Fig. 4. Coordination of Sn atoms in the FE $- Sn_2P_2Se_6$ structure. (a) Se atoms around Sn1, (b) Se atoms around Sn2e.

Let us finally note two interesting points. The first concerns the physical mechanism of the ferroelectric transition. Since the atomic displacements which characterize the ferroelectric phase are located within the volume of thermal agitation above the transition, we attempted also to refine the high temperature structure by assuming the existence of two sites statistically occuped with a 0.5 probability. The result does however not lead to a better R factor. As observed in neutron and Raman experiments the transition is mainly driven by a soft mode, and if an order-disorder component would exist, it would manifest itself only in the vicinity of the phase transition point.

A central peak is indeed observed but the data do not allow to determine whether it is due to a partial order-disorder character of the transition. The second point concerns the symmetry properties of the phases. In the paraelectric phase the inversion operation, acting in the center of the P−P link, relates the Se's. However as we mentioned above, at low temperature the inversion disappears and a distortion of P_2Se_6 is allowed by symmetry, and it is indeed observed to occur. The point symmetry m does not fix either the orientation of the polar displacements of the atoms in the ferroelectric phase. It only requires that the macroscopic resulting polarization P lies within the mirror plane. Structural data reveal indeed that atomic displacements occur in all directions in such a way that the resulting polarization lies in the mirror plane but there clearly exists a component along x outside the error, so that the polarization does not lie along a crystallographic direction. Moreover the component of the displacements in the direction normal to the mirror plane is also significantly non-zero but the corresponding local dipolar moments compensate (these displacements are related by the glide plane) in an antiparallel arrangement.

4 Theoretical aspects

Let us now discuss the phase transition from the paraelectric to the ferroelectric phase in the frame of the phenomenological theory, ignoring the IC phase which will be taken into account in detail in another work. Since the symmetry change involves only a point group reduction, we have to consider the irreducible representations (IR) of point group $2/m$. All of them being unidimensional the order parameter is a single component quantity. However in the low temperature phase with m group, the direction of polarization P is not symmetry-fixed. We are therefore in a somewhat particular situation since we have to consider both components P_x and P_z along the x and z axes defining the mirror plane. Both transform according to the same IR and the first terms in the Landau expansion of the thermodynamic potential are therefore:

$$F = F_0 + \frac{1}{2}\alpha_1 P_z^2 + \frac{1}{2}\alpha_2 P_x^2 + \alpha_3 P_x P_z + \dots \quad (1)$$

Minimizing this expression yields:

$$P_x = -\frac{\alpha_3}{\alpha_2} P_z. \quad (2)$$

Which leads to:

$$F = F_0 + \frac{1}{2}(\alpha_1 - \frac{\alpha_3^2}{\alpha_2}) P_z^2 + \dots \quad (3)$$

This shows that the phase transition if it is second order occurs at T_0 such that $\alpha_1 - \frac{\alpha_3^2}{\alpha_2} = 0$. If we now label Z the coordinate axis along the direction followed by **P** in the neighbourhood of T_0 and X the perpendicular axis lying within the mirror plane, we can write the free energy expansion as:

$$F = F_0 + \frac{1}{2}\alpha_1^* P_Z^2 + \frac{1}{2}\alpha_2^* P_X^2 + \alpha_3^* P_X P_Z + \gamma P_X^3 P_Z + \frac{\beta_1}{4} P_Z^4 + \frac{\beta_2}{4} P_X^2 + \dots \quad (4)$$

where it appears using (1), (2), and (3), that coefficients α_1^* and α_3^* are zero at T_0 and:

$$\alpha_1^* = \frac{(\alpha_1 - \frac{\alpha_3^2}{\alpha_2})}{(1 + \frac{\alpha_1^2}{\alpha_3^2})} = a_1(T - T_0), \alpha_3^* = a_3(T - T_0) \quad (5)$$

α_2^*, β_1, and β_2 are considered as positive constants.

Minimizing (4) with respect to P_X gives the dependence of this last quantity with respect to P_Z in the neighbourhood of T_0 as:

$$P_X = -\frac{\alpha_3^*}{\alpha_2^*} P_Z - \frac{\gamma}{\alpha_2^*} P_Z^3 \dots \quad (6)$$

Replacing this value in (4) and minimizing the obtained expression provides the equilibrium value of P_Z in the neighbourhood of T_0:

$$P_Z \simeq \pm\sqrt{\frac{-a_1(T - T_0)}{\beta_1}} \quad (7)$$

which allows to deduce the temperature dependence of P_X from (5, 6):

$$P_X = \mp\left\{\frac{\alpha_3^*}{\alpha_2^*}\sqrt{\frac{-a_1(T - T_0)}{\beta_1}} + \frac{\gamma}{\alpha_2^*} P_Z^3 (\frac{-a_1(T - T_0)}{\beta_1})^{\frac{3}{2}}\right\} \sim (T - T_0)^{\frac{3}{2}}. \quad (8)$$

Far from T_0 it follows then that there are displacements with components along X in good agreement with the experimental results presented above. However further studies are necessary to check if the temperature dependence expressed by equation (8) is followed.

In fact the expression for the thermodynamic potential is more complicated than the above expression (4) which cannot account for the existence of the intermediate IC-phase. Moreover the negative sign of the quartic term should be taken into account in a more complete theory which should deal with an energy expansion up to order 6. Here the IC-phase is of type II (there is no Lifshitz invariant, the order parameter being a single component quantity) and the softening at $q \neq 0$ is due to a coupling between the order parameter gradient and the strain. The terms $u_{xz}\frac{\partial P}{\partial x}$ and $u_{xz}\frac{\partial P}{\partial z}$ are indeed invariant and are present in the Landau-Ginzburg expansion of F with some coefficients μ_1 and μ_2. They correspond to a coupling between soft and acoustic phonon branches.

The coupling being strong enough the IC-phase appears and the above terms induce a modulation with a wave vector lying in the mirror plane, with q_x and q_z components.

This means that the domain texture of the IC phase, in which the modulation is described by a sequence of ferroelectric domains and parallel domain walls, is built from walls containing Y and rotated away from the z-direction. The electrostatic energy of this texture is minimum when the wave vector lies in the direction perpendicular to $\mathbf{P}$ because walls do not then carry electrical charges (div $\mathbf{P} = 0$). From this it follows that the deviation of $\mathbf{P}$ with respect to the crystallographic axis is expected to be of the same order as the deviation of the modulation vector $\mathbf{q}$, which is consistent with our experimental results. The treatment of the full energy expansion including gradient terms and strains, together with the analysis of the domain texture, will be given in another paper.

5 Conclusion

The change of structure occurring in $Sn_2P_2Se_6$ between the paraelectric and ferroelectric phases has been determined accurately. It appears that the displacements are of the same nature as those taking place in the isomorphous compound $Sn_2P_2S_6$. The comparative study of the PE and FE structures evidences the key-role of the stereoactivity of the Sn^{2+} lone pair in the origin of the structural instability. The ferroelectricity of these materials is connected mainly with atomic displacements lying in the z-direction. Nevertheless there exists a small component of polar displacements in the perpendicular direction with a different temperature variation, as can be obtained from theory. Further studies are necessary to check this point. The present experimental results are also consistent with a mainly displacive nature of the transition since attempts to refine the paraelectric structure with two sites occupancy close to each other did not give better results. Nevertheless since the displacements connected with ferroelectricity lie within the ellipsoid of thermal motion in the paraelectric phase, a slight order-disorder character in the close neighbourhood of the transition point cannot be completely excluded from the structure data.

The authors thank A.P. Levanyuk for useful exchanges concerning the phenomenological theory.

References

1. Yu.M. Vysochanskii, V.Yu. Slivka, Sov. Phys. Usp. **35**, 123 (1992).
2. Yu.M. Vysochanskii, M.M. Maior, V.M. Rizak, V.Yu. Slivka, M.M. Khoma, Sov. Phys. JETP **68**, 782 (1989).
3. T.K. Barsamian, S.S. Khasanov, V.Sh. Shekhtman, Yu.M. Vysochanskii, V.Yu. Slivka, Sov. Phys. Solid State **27**, 2003 (1986).
4. T.K. Barsamian, S.S. Khasanov, V.Sh. Shekhtman, Ferroelectrics **138**, 63 (1993).
5. Yu.M. Vysochanskii, V.Yu. Slivka, A.P. Buturlakin, M.I. Gurzan, D.V. Chepur, Sov. Phys. Solid State **20**, 49 (1978).
6. S.W.H. Eijt, R. Currat, J.E. Lorenzo, S. Katano, P. Saint-Grégoire, B. Hennion, Yu.M. Vysochanskii, Ferroelectrics **202**, 121 (1997).
7. A.I. Ritus, N.S. Roslik, Yu.M. Vysochanskii, A.A. Grabar, V.Yu. Slivka, Sov. Phys. Solid State **27**, 1337 (1985).
8. G. Dittmar, H. Scheaffer, Z. Naturforsch **29**, 312 (1974); C.D. Carpentier, R. Nitsche, Mat. Res. Bull. **9**, 401 (1974).
9. F. Scott, M. Pressprich, R.D. Villert, D.A. Cleary, J. Solid State Chem. **96**, 294 (1992).
10. Yu.V. Voroshilov, M.V. Potorii, L.A. Sejkovskaja, A.V. Yatsenko, I.P. Prits, Sov. Phys. Crystallogr. **33**, 761 (1988).
11. R. Israël, R. de Gelder, J.M. Smits, P.T. Beurskens, S.W. Eijt, Th. Rasing, H. van Kempen, M.M. Maior, S.F. Motrija, Zeitschrift für Kristallographie **213**, 34 (1998).
12. Yu.M. Vysochanskii, V.Yu. Slivka, Yu.V. Voroshilov, M.I. Gurzan, D.V. Chepur, Sov. Phys. Solid State **21**, 1382 (1979).
13. C.D. Carpentier, R. Nitsche, Mat. Res. Bull. **9**, 401 (1974).
14. A.C.T. North, D.C. Phillips, F.S. Matthews, Acta Cryst. A **24**, 351 (1968).
15. D.T. Cromer, D. Liberman, *International Tables for X-Ray Crystallography* (Kynoch Press, Birmingham, UK, 1974), Vol. 4.
16. G.M. Sheldrick, SHELXL96, Program for the refinement of crystal structures, University of Gottingen, Germany (1996).
17. M.N. Burnett, C.K. Johnson, ORTEP III, Report ORNL **6895**, Oak Ridge National Laboratory, Oak Ridge, TN (1996).
18. E.J. Banda, R.A. Craven, R.D. Parks, P.M. Horn, M. Blume, Solid State Commun. **17**, 11 (1975).
19. W. Kleemann, F.J. Schäfer, J. Nouet, J. Phys. C **14**, 4447 (1981) and references therein.
20. J. Galy, G. Meunier, S. Andersson, A. Astrom, J. Solid State Chem. **3**, 142 (1975).
21. J. Galy, R. Enjalbert, J. Solid State Chem. **44**, 1 (1982).